Progress In Electromagnetics Research, Vol. 120, 513–533, 2011

DESIGN OF BROADBAND CIRCULARLY POLARIZED SQUARE SLOT ANTENNA WITH A COMPACT SIZE

J.-Y. Sze* **and S.-P. Pan**

Department of Electrical and Electronic Engineering, Chung Cheng Institute of Technology, National Defense University, 190 Sanyuan 1st. St., Dasi Township, Taoyuan County 33508, Taiwan, R.O.C.

Abstract—This paper proposes a newly designed compact coplanar-waveguide-fed wideband circularly polarized (CP) printed square slot antenna (PSSA), in the square slot of which are a halberd-shaped feeding signal line and a square ring patch. By placing a specially designed metal reflector behind the bidirectional CP PSSA, one can obtain unidirectional CP patterns with a associated 3-dB axial-ratio bandwidth (ARBW) almost the same as that of the bidirectional antenna. The bidirectional *L*- and *S*-band PSSAs designed on FR4 substrates have 3-dB ARBWs as large as 25.3% and 29.1%, respectively. For the *L*-band antennas, the unidirectional design yields a 3-dB ARBW of 25.7% and a gain of about 3 dB higher than that of the bidirectional counterpart. In all these 3-dB axial-ratio bands, impedance matching with VSWR ≤ 2 is also achieved. Most importantly, the design concepts, procedures, and rules for the proposed antenna are presented in detail.

1. INTRODUCTION

With booming wireless-communication technologies, many satellite systems for global-navigation applications or communication applications [1, 2] have been made commercially available. To simultaneously support several satellite systems whose operating bands are closely spaced, large 3-dB axial-ratio bandwidths (ARBWs) are required for the antennas to be devised. Many popular circularly polarized (CP) patch antennas [3–7] and loop antennas [8, 9] have narrower CP bandwidths of less than 20%. Known not only for their compactness and low-profile features but also for their easily attained large CP bandwidths using simple design technologies and constructions, printed slot

Received 1 July 2011, Accepted 26 September 2011, Scheduled 11 October 2011

* Corresponding author: Jia-Yi Sze (szejy@ndu.edu.tw).

antennas have received much attention in recent years [10–22]. Among these antenna designs, the CP ring slot antennas in [10–12] still have CP bandwidths of less than 25% even though many CP-bandwidth-enhancement efforts have been made. The remaining ones are regarded as wideband CP antennas, whose 3-dB ARBWs are all larger than 25% with respect to the center frequencies of their 3-dB axial-ratio (AR) bands (or alternatively called CP bands for short). For comparison, the 3-dB ARBWs and antenna sizes of these wideband antennas are summarized in Table 1. In this table, f_L is the lower-edge frequency of the CP band, and λ_L is the corresponding free-space wavelength. The slot area (the antenna area) is the area of the smallest rectangle that can enclose the slot (the entire low-profile antenna). Note that the slot and antenna areas are measured in λ_L instead of the free-space wavelength λ_0 at the CP-band center frequency f_0 because for two wideband CP antennas having the same f_L but different f_0, the one with a wider CP band will have a larger electric size if λ_0 is chosen as the reference. Choosing λ_0 as the reference will result in somewhat unfair size comparison between the two wideband CP antennas. In fact, if λ_L is chosen as the reference instead, the wider-band CP antenna will be of the same size as that of the narrower-band CP antennas.

The simple antenna designs in [13–15] have a circular slot or a triangular slot fed by a closely coupled L-shaped microstrip line. Although the 3-dB ARBWs of these slot antennas are as large as 31% to 45%, their normalized antenna areas are comparatively large (larger than $0.7\lambda_L^2$) and cannot be reduced if the 3-dB ARBWs are to be maintained because reducing the ground-plane size (and hence the antenna area) would raise the lower-edge frequency of an antenna's CP band, thus significantly shrinking the CP bands and shifting up the associated CP-band center frequencies. In addition, their normalized slot areas are larger than $0.1\lambda_L^2$. The antenna designs in [16, 17] with an L-shaped coupled feedline and embedded stub(s) in the slot regions have smaller antenna areas than those in [13–15] while still having large slot areas.

To overcome the drawbacks (i.e., large antenna or slot area, or both) of the above slot antennas which are all fed by microstrip lines, many broadband CP slot antennas with new design strategies have been developed [18–22]. In particular, these antennas are all fed by co-planar waveguides (CPWs). The antenna design proposed in [18] employed an inverted-L-shaped signal line of the CPW fed from a corner of a square slot and an additional pair of grounded strips in the slot. The antenna designs proposed in [19, 20] are fed by a widened signal line of the CPW. Two grounded inverted-L metallic strips [19] or two grounded square patches with E-shaped slits [20] are placed around

Table 1. CP bands and sizes of some existing wide-slot antennas.

ref.	f_L (MHz)	f_C (MHz)	3-dB ARBW (%)	Slot area (mm × mm), (λ_L^2)	Ant. area (mm × mm), (λ_L^2)
[13]	2910	3735	44.2	37.6×37.6, 0.133	100×100, 0.941
[14]	2700	3200	31	40×34.64, 0.112	100×100, 0.81
[15]	2570	3320	45	40×40, 0.117	100×100, 0.734
[16]	2700	3400	41.2	58×58, 0.272	82×81, 0.538
[17]	2600	3475	50.4	$> 62 \times 58$, > 0.27	82×81, 0.5
[18]	1880	2220	30.6	40×40, 0.063	60×60, 0.141
[19]	2065	2413	28.8	40×40, 0.076	60×60, 0.171
[20]	1739	2088	33.4	40×40, 0.054	60×60, 0.121
[21]	2075	2745	48.8	40×40, 0.077	60×60, 0.172
[22]	2150	2900	51.7	40×40, 0.082	60×60, 0.185

two opposite corners of the slot [20]. The feeding structures of the antenna designs in [19, 20] were later replaced by a lightening-shaped signal line. The resulting antennas in [21] and [22] possess a greatly enhanced CP bandwidth of up to 48.8% and 51.7%, respectively. In addition, the normalized antenna and slot areas are relatively small and less than $0.2\lambda_L^2$ and $0.09\lambda_L^2$, respectively.

In this paper, we propose a method for designing a new broadband CP PSSA with compact antenna and slot sizes. Similar to that in [18], the design of the proposed antenna also employs an inverted-L-shaped signal line of the CPW fed from a corner of a square slot. However, the grounded strips in the slot have been replaced by non-grounded square ring patch. It will be demonstrated that, if a specially designed novel

metal reflector is placed behind, the new CP PSSA can be further developed to suppress the backward radiation and hence to increase the antenna gain. Most importantly, the design concepts, procedures, and rules for the proposed antenna will be systematically elucidated in detail.

2. ANTENNA CONFIGURATION

Figure 1(a) shows the geometry of the proposed CP PSSA, which is fabricated on a square microwave substrate with side length G, thickness h, dielectric constant ε_r, and loss tangent $\tan\delta$. A square slot of side length L_s is symmetrically etched from the ground plane printed on one side of the substrate. The antenna is fed from the lower-right corner of the square slot by a 50-Ω CPW with a w_f-wide signal line and two g-wide gaps. The CP operation is mainly attributed to two structures, one being a specially designed feeding structure and the other a square ring patch implanted in the slot region. The feeding structure consists of two w_1-wide strip sections oriented in the x and y directions that are connected to the signal line of the corner-fed CPW and protruded into the square slot. The two strip sections are g-distance away from the left, right, and lower edges of the square slot. For convenience, refer to the strips that are protruded into the slot from the CPW feedline as a feeding signal line. The feeding signal line of the proposed antenna (see Fig. 1(a)) is then of halberd shape. This halberd-shaped feeding signal line will be seen later to account for the CP operation in the high-frequency portion of the designed CP band. On the other hand, the CP operation in the low-frequency

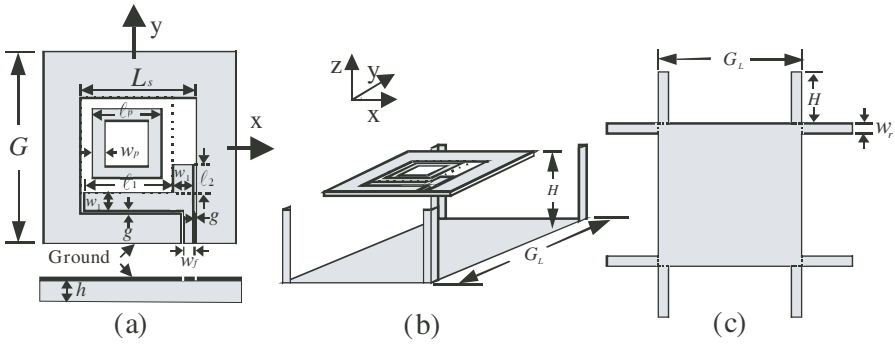

Figure 1. (a) Configuration of the proposed bidirectional CP slot antenna. (b) Configuration of the proposed unidirectional CP slot antenna. (c) Antenna reflector with side walls.

portion is mainly governed by the square ring patch with width w_p and outer side length ℓ_p. As shown in Fig. 1(a), the square ring patch is symmetrically implanted in the square slot region formed by the upper edge of the x-directed strip and the left edge (denoted by the dotted line in Fig. 1(a)) of the y-directed strip of the halberd-shaped feeding structure and the left and upper edges of the L_s-wide square slot.

In addition, for the purpose of suppressing the backward radiation and hence increasing the antenna gain, a specially designed square metal reflector with side length G_L (see Fig. 1(b)) is placed at a distance of roughly $\lambda_0/4$ behind the substrate, where λ_0 is the free-space wavelength at the center frequency of the CP band. This reflector is designed to reflect the $-z$-directed wave due to the main radiator into the $+z$-directed wave so that this reflected wave possesses the same polarization and phase as those of the $+z$ directed radiation due to the main radiator alone. Attached at the two ends of each side of the square reflector are vertical walls with width w_r and height H. Note that the ground plane covering the substrate coincides with the plane containing the upper edges of the vertical walls.

3. CONCEPTS AND PROCEDURE OF ANTENNA DESIGN

Note that most CP antennas in [13–22] are designed to operate in S band (2–4 GHz). For comparison with those antennas in terms of antenna gains and ARBWs, the antenna design procedures to be developed in this study will also use an S-band CP PSSA as an example. Once established, these procedures will be verified by designing an additional L-band antenna. To systematically elucidate the design methods and principles, we use a CPW-fed PSSA operating at 2600 MHz as the reference antenna. For the ease of fabrication and discussion, all the antennas presented in this study adopt the same commercially available FR4 substrates with $\varepsilon_r = 4.4$, $\tan\delta = 0.019$, and $h = 1.6$ mm. The 50-Ω CPW then has the dimensions of $w_f = 5$ mm and $g = 0.5$ mm.

3.1. Slot Dimensions of CPW-fed CP PSSA

Because analytic formulas relating the dimensions and resonant frequencies of a square slot etched from a finite ground plane are not available, we will first base on extensive simulations using Ansoft HFSS to determine an empirical formula relating the slot size of the reference antenna to the fundamental-mode resonant frequency for certain ratios of L_s to G. For a CPW-fed LP PSSA, its fundamental-mode resonant

frequency depends not only on the side length of the slot but also on the ground-plane size. We found that with the ratio L_s/G in the range of 0.5–0.6, the resonant frequency and the side length of the slot are approximately related by

$$f_r \approx \frac{c_0}{2(L_s + w_f)\sqrt{\varepsilon_{eff,1}}}, \quad \varepsilon_{eff,1} = \frac{1+\varepsilon_r}{2} \tag{1}$$

where c_0 is the speed of light in vacuum and $\varepsilon_{eff,1}$ the effective dielectric constant.

Next, in order to acquire a smaller size for the reference antenna operating at 2600 MHz, we choose from the legitimate range for (1), the ratio L_s/G to be 0.6. This leads to $L_s = 30$ mm and $G = 50$ mm according to (1) with $f_r = 2600$ MHz. The HFSS-simulated RL curve for the reference antenna with the signal line of the CPW protruded halfway into the slot is shown in Fig. 2, which reveals that the resonant frequency is 2538 MHz, quite close to the desired 2600 MHz. Note that the reference antenna is a linearly polarized (LP) one.

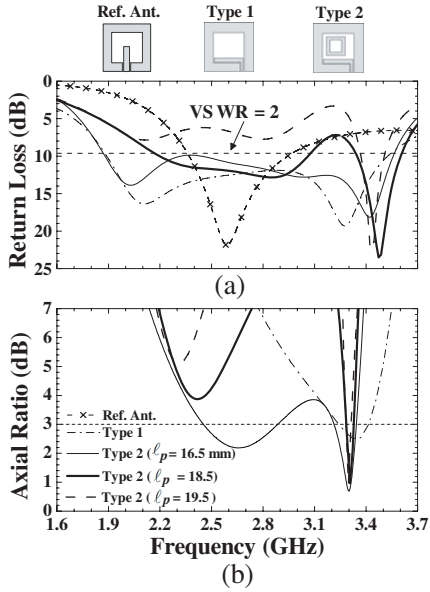

Figure 2. Simulated (a) return loss and (b) axial ratio responses for the reference antenna (linearly polarized), a type 1 antenna, and three type 2 antennas with ($\ell_p = 16.5$, 18.5, 19.5 mm).

3.2. Formation of CP Band at Higher Frequencies (Type 1 Antenna)

From the CP antennas proposed in [13–18], we notice that if the feeding signal line of a PSSA is of L or inverted-L shape, CP radiation can be excited in a certain frequency band. Our CP PSSA design starts with this design concept. Let the protruded strip be a simple x directed line section, which in conjunction with the signal line of the feeding CPW forms an inverted-L feeding signal line. Experience in CP antenna design also suggests to us that various perturbation structures can be implanted in the slot region to excite CP radiation in some different frequency bands. In order to reserve enough space for deploying perturbation structures, the CPW is arranged to asymmetrically feed the square slot. This leads to a CPW-fed PSSA with an inverted-L feeding signal line, as denoted by the type 1 antenna shown in Fig. 2. Simulated RL and AR curves for the type 1 antenna with the x-directed feeding strip section having a width of $w_1 = 5\,\text{mm}$ and a length of $L_s - 2g = 29\,\text{mm}$ are shown in Fig. 2. Two resonant modes of the type 1 antenna are found to resonate at 2120 and 3280 MHz. Their associated VSWR ≤ 2 impedance bands are combined into a single wide impedance band of 1838–3484 MHz. However, only the high-frequency resonant mode possesses CP characteristics. Note that the lowest AR of 2.5 dB occurs at 3324 MHz, which is denoted by f_{H0}. Fig. 3 shows the HFSS-simulated magnetic current distributions of the type 1 antenna at 3324 MHz for the four time instants of $\omega t = 0°$, 90°, 180°, and 270°. With the relatively weak magnetic currents neglected for clearness, plotted in these figures are only the major ones, which are found to flow along the perimeter of the inverted-L feeding signal line. The predominant components of these major magnetic currents at $\omega t = 0°$, 90°, 180°, and 270° are found to be oriented along the x, y, $-x$, and $-y$ directions, respectively. This implies the type 1 antenna in the CP band around f_{H0} produces RHCP radiation in the $+z$ direction. Concluded from extensive simulations, we can empirically relate f_{H0} to the antenna dimensions by

$$f_{H0} \approx \frac{c_0}{[2(L_s - 2g + w_f) + w_1]\sqrt{\varepsilon_{eff,2}}}, \quad \varepsilon_{eff,2} = \frac{2\varepsilon_r}{1 + \varepsilon_r}. \tag{2}$$

3.3. Formation of CP Band at Lower Frequencies (Type 2 Antenna)

The low-frequency resonant mode (around 2120 MHz) produces only LP radiation. To have a wide CP band for the designed antenna, we can try to convert the LP radiation into CP radiation in the lower resonant

band. Fig. 4(a) shows the magnetic current distribution of the type 1 antenna at 2120 MHz. The magnetic currents above the x-directed feeding strip section for the low-frequency resonant mode at 2120 MHz appear to be much stronger than those for the high-frequency resonant mode at 3324 MHz (see Fig. 3). Hence, we can implant a perturbation structure in the slot region above the inverted-L feeding signal line to effectively perturb the magnetic current distribution of the low-frequency resonant mode without severely downgrading the CP characteristics of the high-frequency resonant mode. The perturbation structure can be properly designed to yield CP radiation for the low-frequency resonant mode. A w_p-wide square ring patch with outer side length ℓ_p is found to be a possible perturbation structure that does the job. The square ring patch can be implanted at the center of the square slot region formed by the upper edge of the x-directed strip and the left edge (denoted by the dotted line in Fig. 1(a)) of the y-directed strip of the proposed halberd-shaped feeding structure and the left and upper edges of the L_s-wide square slot. The resulting antenna is referred to as a type 2 antenna.

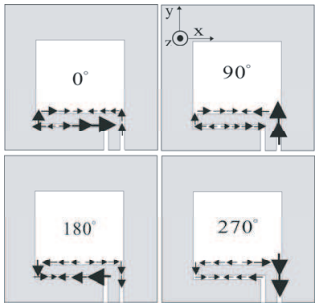

Figure 3. Magnetic current distributions of the type 1 antenna for four different phases at $f_{H0} = 3324$ MHz.

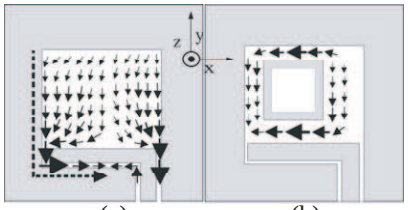

Figure 4. Magnetic current distributions of (a) the type 1 antenna at 2120 MHz and (b) the type 2 antenna with $\ell_p = 18.5$ mm at $f_{L0} = 2400$ MHz.

Simulated RL and AR curves for three type 2 antennas with w_p fixed at 3 mm and ℓ_p chosen to be 16.5, 18.5, and 19.5 mm are shown in Fig. 2. Similar to the type 1 antenna, each type 2 antenna preserves a 3-dB AR band within the high-frequency resonant band, although the 3-dB ARBWs of these antennas may be different. In addition to the high-frequency CP band, a low-frequency CP band can also be observed for each of the three type 2 antennas. Moreover, the larger is the value of ℓ_p, the lower is the frequency (denoted by f_{L0}) at which the AR curve reaches a local minimum in the low-frequency range. The simulated magnetic current distribution for the type 2 antenna with $\ell_p = 18.5$ mm at $f_{L0} = 2400$ MHz and $\omega t = 0^\circ$ is shown in Fig. 4(b). This magnetic current distributions in conjunction with those (not shown here for conciseness) at other time instants implies that the fields radiated in the $+z$ direction around f_{L0} are also of RHCP, the same as the fields around f_{H0}. From extensive simulations, f_{L0} and the antenna dimensions can be empirically related by

$$f_{L0} \approx \frac{c_0}{2(\ell_p + L_s)\sqrt{\varepsilon_{eff,2}}} \tag{3}$$

where $\varepsilon_{eff,2}$ is given in (2). Although f_{L0} decreases with ℓ_p, the low- and high-frequency CP bands start to become disjoint only when ℓ_p is greater than 16.5 mm. Unfortunately, the band separation accompanies deterioration in AR and impedance matching.

3.4. Combination of Two Disjoint CP Bands and AR Optimization (Type 3 Antenna)

Our goal is to design an antenna which has a broad CP band. This goal can be achieved by either raising the low-frequency or lowering the high-frequency CP band so that the two CP bands are close enough to be combined into a single broader one. Recall that the major magnetic currents at f_{H0} flow along the perimeter of the inverted-L feeding signal line. We then expect that f_{H0} can be lowered if the perimeter of the feeding signal line can be properly lengthened. This can be achieved by adding an additional y-directed feeding strip section with width w_1 and length ℓ_2 to the inverted-L feeding signal line of the type 2 antenna with $\ell_p = 18.5$ mm to form a halberd-shaped feeding signal line. The resulting antenna is referred to as a type 3 antenna. Fig. 5 shows the simulated RL and AR curves for $\ell_2 = 0$, 3, and 5 mm (the one with $\ell_2 = 0$ mm is a type 2 antenna). Measured results for $\ell_2 = 5$ mm are also shown in this figure, and they agree reasonably well with simulated ones. The additional y-directed strip section is found capable of effectively lowering the high-frequency CP band. The

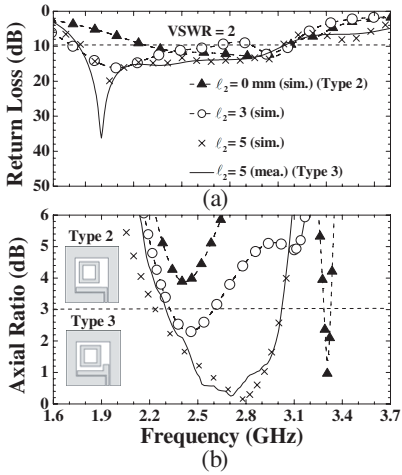

Figure 5. (a) Return loss and (b) axial ratio for three different values of ℓ_2 with $G = 50\,\text{mm}$, $L_s = 30\,\text{mm}$, $w_f = 5\,\text{mm}$, $g = 0.5\,\text{mm}$, $\ell_1 = 24\,\text{mm}$, $\ell_p = 18.5\,\text{mm}$.

empirical formula pertaining to f_{H0} can then be modified as

$$f_{H0} \approx \frac{c_0}{[2(L_s - 2g + \ell_2 + w_f) + w_1]\sqrt{\varepsilon_{eff,2}}} \tag{4}$$

Observe that the decrease of f_{H0} goes along with a slight increase of f_{L0}. This phenomenon can be explained by the fact that the region allowing the magnetic current to flow around the square ring patch at f_{L0} (see Fig. 4(b)) is squeezed because of the presence of the y-directed strip section in the halberd-shaped feeding signal line. The equivalently slightly shortened route of the magnetic current distribution thus leads to a slightly increased f_{L0}. In the meantime, with $\ell_2 = 5\,\text{mm}$ chosen for the type 3 antenna, the AR performance is greatly improved in the combined broader CP band with a measured (simulated) minimum AR of 0.3 dB (0.09 dB) at 2705 MHz (2785 MHz). The measured 3-dB AR band of 2300–3020 MHz corresponds to a 3-dB ARBW of 27.1% with respect to the center frequency 2660 MHz. Note that the measured CP-band center frequency of this type 3 antenna is very close to the impedance-band center frequency of the reference antenna. Obviously, the characteristics of the proposed antenna design are to transform the LP reference antenna in a broad band around the impedance-band center frequency into a CP antenna. Because the $+z$-directed waves are both RHCP in the two originally disjoint CP bands, the $+z$-directed waves in the combined broader CP band are also RHCP.

In the design process from the type 1 antenna, through the type 2 antenna, finally to the type 3 antenna, we are able to achieve our design goal because various substructures in the antenna contribute more or less to the two conditions required for CP operation: nearly equal amplitude for two orthogonal transverse far fields and approximately 90° phase difference between them. Besides the ARs, Fig. 6 shows for the three different types of antennas the HFSS-simulated amplitude ratios (i.e., E_x/E_y) of two orthogonal far fields in the $+z$ direction and the simulated phase differences (PDs) between the two fields. The type 1 antenna produces a far-field amplitude ratio of −2 dB and a PD of 90° at 3324 MHz. The resulting AR appears to be the smallest around the type 1 antenna's high-frequency CP band. The two local minimum ARs for the type 2 antenna occurs at 2417 and 3306 MHz, at which the amplitude ratios (phase differences) are 4 dB (98°) and 2 dB (90°), respectively. Compared with the types 1 and 2 antennas, in general the type 3 antenna's amplitude ratios are closer to 0 dB, and the associated phase differences are also very close to 90°, resulting in a broader CP band and in this band a smaller minimum AR. This type 3 antenna hence is our proposed S-band CP PSSA.

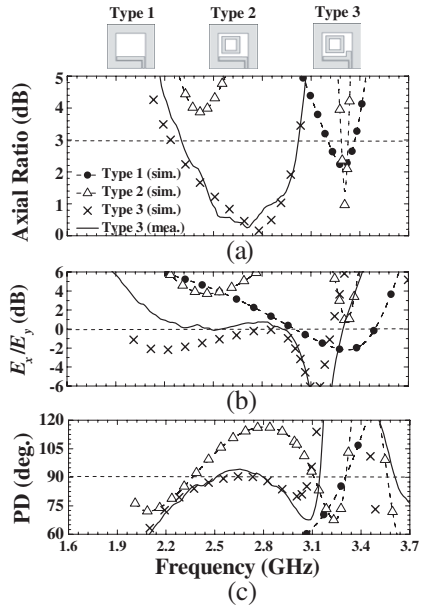

Figure 6. (a) Axial ratio, (b) amplitude ratio, and (c) phase difference for the three different types of S-band antennas.

3.5. More Design Prototypes for Broadband *S*-band CP PSSAs

Note that ℓ_p is one of the parameters determining the location of the low-frequency CP band. Hence, with the sizes of G and L_s fixed, we observe that to a certain extent a larger ℓ_p gives a lower location of the low-frequency CP band. If a larger ℓ_p is selected with ℓ_2 appropriately adjusted such that a combined broad CP band can still be obtained around a lower frequency location, antenna miniaturization can be achieved by controlling ℓ_p. That is, if G and L_s are fixed, we may explore whether the center frequency of the broad CP band can be lowered by increasing ℓ_p; conversely, if the center frequency of the broad CP band is preselected, we may check whether a smaller antenna size (i.e., smaller G and L_s) can be obtained by selecting a larger ℓ_p. In this subsection, four different CP PSSA prototypes with $\ell_p =$ 16.5, 18.5, 19.5, and 20.5 mm are developed using the proposed design procedures. Besides verifying the design procedures, the purpose is to find to what extent the antenna can be miniaturized. Measured results for these four antennas shown in Fig. 7 indicate that with ℓ_p in between $0.7\,(L_s - w_1 - g)$ and $0.8\,(L_s - w_1 - g)$, a combined broad CP band can always be obtained through adjusting ℓ_2. Among these four antenna prototypes, the one with $\ell_p = 19.5$ mm has the largest 3-dB ARBW of 29.1% with respect to 2.52 GHz, the center frequency of the combined CP band of 2155–2890 MHz. This CP band is completely enclosed by the associated impedance band of 1714–2904 MHz (51.5%).

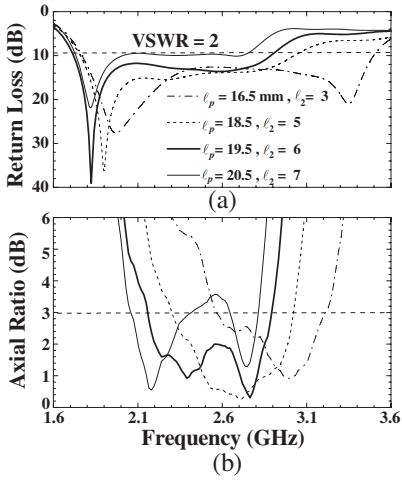

Figure 7. Measured (a) return loss and (b) axial ratio for four type 3 antennas with different values of ℓ_p and the associated optimized ℓ_2.

When the type 3 antenna with $\ell_p = 16.5\,\text{mm}$ is smaller than $0.7\,(L_s - w_1 - g)$, the center frequency of the 3-dB AR band is shifted from the resonant frequency (2600 MHz) of the LP CPW-fed slot antenna to a higher one, a result not as expected. For the antenna prototype with $\ell_p = 20.5\,\text{mm}$, which is greater than $0.8\,(L_s - w_1 - g)$, a combined broad CP band can no longer be achieved because the low-frequency CP band has been lowered too much such that it is too far away from the high-frequency counterpart. Furthermore, the impedance matching becomes worse, and the two disjoint CP bands cannot be completely covered by the associated impedance band. Relevant measured results are summarized in Table 2.

4. DESIGN OF AN *L*-BAND CP PSSA

On the basis of the design concepts and procedures developed so far, we will further design an L-band (1–2 GHz) broadband CP PSSA for verification. First, we will design a bidirectional broadband L-band CP PSSA. Second, it may sometimes be desirable that the bidirectional radiation pattern of the CP PSSA just designed is transformed into a unidirectional one. For that purpose, one can place a specially designed square reflector at a distance of about $\lambda_0/4$ behind the substrate. The same FR4 substrates will be adopted in the design. Results obtained in the course of the design are presented below.

Table 2. Structural parameters, measured 3-dB ARBWs, and measured VSWR $\leq$ 2 impedance bands of the prposed Antennas; $\varepsilon_r = 4.4$, $\tan\delta = 0.019$, $h = 1.6\,\text{mm}$, $w_f = 5\,\text{mm}$ and $g = 0.5\,\text{mm}$. f_c refers to the center frequency of the 3-dB AR band. (unit: mm).

H	G_L	G	L_s	w_1	w_p	ℓ_p	ℓ_1	ℓ_2	Impedance BW MHz, %	f_c GHz	3dB ARBW MHz, %	Gain (dBic)
∞	–	50	30	5	3	16.5	24	3	1743, 66.2% (1763–3506)	2.89	645, 22.3% (2570–3215)	4.5
∞	–	50	30	5	3	18.5	24	5	1297, 54% (1753–3050)	2.66	720, 27.1% (2300–3020)	4.3
∞	–	50	30	5	3	19.5	24	6	1214, 51.5% (1714–2904)	2.522	735, 29.1% (2155–2890)	4.0
∞	–	105	63	10	15	42	52	11	834, 64.8% (870–1704)	1.345	340, 25.3% (1175–1515)	3.9
55.8	140	105	63	10	15	42	52	7.5	680, 49.6% (1032–1712)	1.40	360, 25.7% (1220–1580)	6.8

4.1. Design of CP PSSA with Bidirectional Radiation

To verify the design procedures presented in Section 3, we will design an L-band CP PSSA with a purposely pre-determined CP-band center frequency of 1350 MHz. This frequency is very close to half of the CP-band center frequency of 2660 MHz and to half of the minimum-AR frequency of 2705 MHz of a previously designed type 3 S-band CP PSSA presented in Section 3.4. With $f_r = 1350$ MHz, we have $L_s \approx 62.6$ mm according to (1). For convenience, we round up the size to an integer value, i.e., $L_s \approx 63$ mm. With $L_s/G = 0.6$ assumed, we have $G = 105$ mm, which is also of integer value. Other structural dimensions in the design process are obtained as $w_1 = 10$ mm for the type 1 antenna, $\ell_p = 42$ mm and $w_p = 15$ mm for the type 2 antenna, and $\ell_2 = 11$ mm for the type 3 antenna. Measured RL and AR curves of these three antennas are shown in Fig. 8. As expected, the type 3 antenna performs best. Its measured 3-dB AR band of 1175–1515 MHz (25.3% with respect to the center frequency 1345 MHz) is completely enclosed by the associated VSWR ≤ 2 impedance band of 870–1704 MHz (64.8% with respect to the center frequency 1287 MHz). Note that the CP-band center frequency is surprisingly close to the desired one. Also shown in Fig. 8 are the simulated results of the type 3 antenna, which agree well with the measured data. In addition,

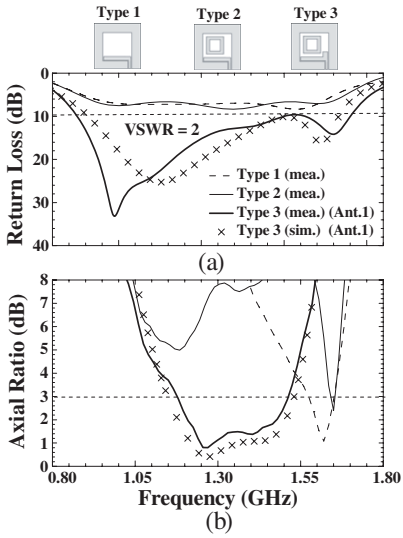

Figure 8. (a) Return loss and (b) axial ratio for the three types of L-band antennas designed using the procedures developed in Section 3.

note that the evolution of the CP characteristics of the three L-band antenna prototypes is rather similar to that for the three S-band ones.

4.2. Design of CP PSSA with Unidirectional Radiation

Antennas radiating into only one half-space are preferred for some applications. In this subsection, we will add a reflector to the optimal L-band CP PSSA (i.e., the type 3 antenna) developed in Section 4.1 in an attempt to acquire single broadside radiation. The radiation due to the reflector-free CP PSSA is RHCP in the $+z$ direction and LHCP in the $-z$ direction. To suppress the backward ($-z$ directed) radiation and hence to increase the antenna gain, the simplest way is to place a G_L-wide square reflector at a distance of $H = \lambda_0/4$ below the ground plane of the main radiator, where λ_0 is the free-space wavelength at 1345 MHz. This leads to $H = 55.8$ mm. Extensive simulations revealed that the reflector somewhat degrades the CP performance. In general, the smaller is the value of G_L, the smaller is the 3-dB ARBW. As long as G_L is greater than $5\lambda_0/8$, a CP band with an AR of less than 3 dB can still be obtained. However, if $G_L = 120$ mm (which is only slightly smaller than $5\lambda_0/8$) is selected, the minimum AR in the L band degrades to 4 dB. In order not to increase the overall antenna size, we fixed G_L at 140 mm ($5\lambda_0/8$). We found that in this case the structural parameter ℓ_2 can be adjusted again to improve the CP performance. However, the largest 3-dB ARBW that can be obtained is only 16.8% (1365–1615 MHz) even with ℓ_2 adjusted to 7.5 mm. Simulated results of this antenna shown in Fig. 9 correspond to the case of $w_r = 0$ mm. Such a greatly reduced 3-dB ARBW is roughly two-thirds of that of the reflector-free type 3 antenna presented in the previous subsection.

Nevertheless, the CP performance can still be improved without increasing G_L. If a vertical side wall is attached to each edge of the square reflector, the CP performance can be changed. Reflectors with side walls of many different heights have been simulated using Ansoft HFSS (the results are not shown here for conciseness). Among them, the side walls with a height of 55.8 mm (which is the same as H) were observed to result in the best CP performance. Hence, assume that the height of the side walls is H for the rest of the discussion. Comparing the two sets of curves associated with $w_r = 0$ and 70 mm shown in Fig. 9, the former corresponds to the case where there is no side wall at all, and the latter pertains to the case where the side walls completely surround the square reflector since in this case $w_r = G_L/2$ (see Fig. 1). The antenna with complete side walls has an orthogonal far-field amplitude ratio (E_x/E_y in the z direction) of 0 dB at 1272 MHz and a PD of 90° at 1310 MHz. The amplitude-ratio and PD curves are fast varying around these two frequencies, resulting in

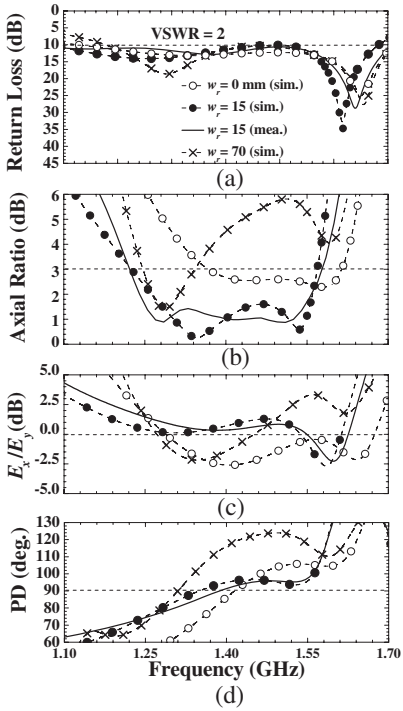

Figure 9. (a) Return loss, (b) axial ratio, (c) amplitude ratio, and (c) phase difference for the L-band antennas with different side walls.

a CP band of only 1245–1340 MHz. On the other hand, the antenna without any side walls has an E_x/E_y ratio of -0.43 dB at 1563 MHz and a PD of 90° at 1415 MHz. Because the amplitude-ratio and PD curves are relatively slowly varying in between these two frequencies, the resulting CP band (1365–1615 MHz) is relatively wide. Note that these two CP bands are disjoint but very close to each other. One may then expect that there exists a compromising reflector structure between the reflector with complete side walls and the one without any side walls such that the two CP conditions (E_x/E_y close to 0 dB and PD close to 90°) can be obtained in both of the disjoint bands. From this design concept and through some simulations, we found that a reflector with partially covered side walls is indeed a compromising reflector structure making the design goal achieved. With w_r selected to be 15 mm, which implies that two pieces of $15 \times 55.8\,\text{mm}^2$ metals are attached at the two ends of each side of the square reflector (see Fig. 1), a broad 3-dB AR band of 1220–1580 MHz (25.7% with respect to the

center frequency 1400 MHz) is obtained and completely covered by the impedance band of 1032–1712 MHz (49.6%). The measurement agrees well with the simulation. The measured CP-band center frequency (1400 MHz) is slightly higher than that (1345 MHz) of the reflector-free CP PSSA. The phenomenon that the CP-band center frequency is slightly increased after the reflector is added can also be observed in [14]. Moreover, the 3-dB ARBW (25.3%) for the reflector-free antenna is approximately the same as that (25.7%) of the one with a partial-side-wall reflector. Relevant measured data of these two antennas are also summarized in the last two rows of Table 2.

4.3. Radiation Patterns and Gains for the Unidirectional CP PSSA

The far-field radiation patterns of the reflector-backed L-band CP PSSA with $w_r = 15$ mm in both xz and yz planes at 1290 and 1510 MHz were measured by using the NSI-800F-10 far-field antenna measurement system. As shown in Fig. 10, the antenna produces RHCP waves in the $z > 0$ half-space, near the $+z$ direction of which the radiation fields have larger RHCP-to-LHCP ratios and hence

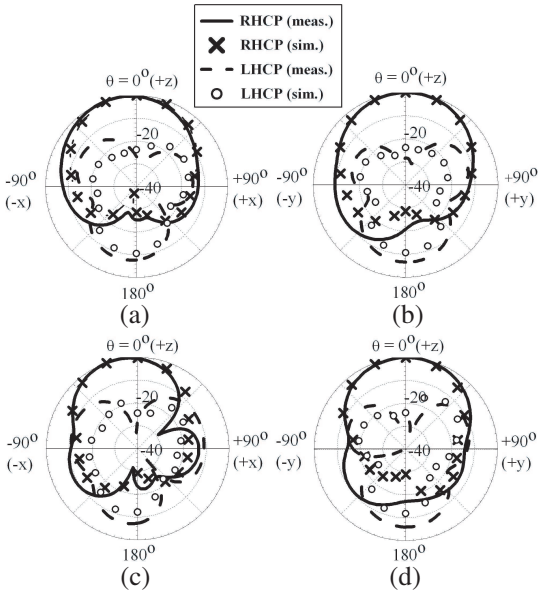

Figure 10. Far-field patterns in the xz and yz planes for the reflector-backed L-band antenna with partially covered side walls ($w_r = 15$ mm) at 1290 MHz ((a) and (b)) and at 1510 MHz ((c) and (d)).

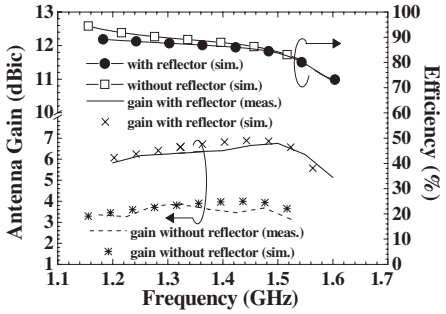

Figure 11. Antenna gains in the +z direction and efficiencies for the L-band reflector-free antenna ($\ell_2 = 11\,\text{mm}$) and reflector-backed antenna ($\ell_2 = 7.5\,\text{mm}$).

smaller ARs. The measurement agrees quite well with the simulation, especially for the RHCP waves in the $z > 0$ half-space. In the measured data for both 1290 and 1510 MHz, the forward ($+z$ directed) RHCP wave is at least 19 dB larger than the backward ($-z$ directed) RHCP wave and 8 dB larger than the backward LHCP wave. In the $+z$ direction, the LHCP field is $-26.5\,\text{dB}$ ($-30\,\text{dB}$) relative to the RHCP field at 1290 MHz (1510 MHz), corresponding to an AR of 0.9 dB (0.87 dB), which agrees with that shown in Fig. 9. Fig. 11 shows in the 3-dB AR bands the measured and simulated antenna gains in the $+z$ direction and the simulated efficiencies for two L-band CP PSSAs, one without a reflector ($\ell_2 = 11\,\text{mm}$) and the other with a partial-side-wall reflector ($\ell_2 = 7.5\,\text{mm}$ and $w_r = 15\,\text{mm}$). The former antenna has less gain than the latter by roughly 3 dB in the frequency range of interest, with a maximum gain of 3.9 dBic for the former and 6.8 dBic for the latter. In addition, the simulated efficiencies for both antennas are above 80% for most of the frequency range of interest.

5. CONCLUSIONS

Design procedures have been developed for designing a broadband CP PSSA by using an S-band antenna as an example. A similar process has been applied to design an additional L-band CP PSSA to verify the design procedures, which have been found easy to follow. The occupied normalized antenna (slot) area is $0.129\lambda_L^2$ ($0.046\lambda_L^2$) for the S-band antenna and $0.169\lambda_L^2$ ($0.06\lambda_L^2$) for the reflector-less L-band antenna. Both antennas possess a 3-dB ARBW of more than 25% with the corresponding 3-dB AR band completely enclosed in the associated VSWR $\leq$ 2 impedance band. Finally, with a specially

designed reflector placed behind the L-band antenna, the antenna gains are increased by a factor of 3 dB. This antenna with unidirectional radiation has a CP band of 1220–1580 MHz.

ACKNOWLEDGMENT

The authors would like to thank the reviewers for their careful review and valuable suggestions. This work was supported by the National Science Council of Taiwan, ROC, under Grand NSC 97-2221-E-606-024.

REFERENCES

1. Samper, J. M., R. B. Pérez, and J. M. Lagunilla, *GPS & Galileo: Dual RF Front-end Receiver And Design, Fabrication, and Test*, McGraw-Hill, New York, 2009.
2. Johnson, R. C. and H. Jasik, *Antenna Engineering Handbook*, McGraw-Hill, New York, 1984.
3. Yang, S. S., K.-F. Lee, A. A. Kishk, and K.-M. Luk, "Design and study of wideband single feed circularly polarized microstrip antennas," *Progress In Electromagnetics Research*, Vol. 80, 45–61, 2008.
4. Lai, C.-H., T.-R. Chen, and T.-Y. Han, "Circularly-polarized reconfigurable microstrip antenna," *Journal of Electromagnetic Waves and Applications*, Vol. 23, No. 2–3, 195–201, 2009.
5. Kasabegoudar, V. G. and K. J. Vinoy, "A broadband suspended microstrip antenna for circular polarization," *Progress In Electromagnetics Research*, Vol. 90, 353–368, 2009.
6. Lin, C., F.-S. Zhang, Y. Zhu, and F. Zhang, "A novel three-fed microstrip antenna for circular polarization application," *Journal of Electromagnetic Waves and Applications*, Vol. 24, No. 11–12, 1511–1520, 2010.
7. Chen, X., G. Fu, S.-X. Gong, Y.-L. Yan, and J. Chen, "Parametric studies on the circularly polarized stacked annular-ring microstrip antenna," *Progress In Electromagnetics Research C*, Vol. 12, 65–77, 2010.
8. Tsai, C.-L., S.-M. Deng, C.-K. Yeh, and S.-S. Bor, "A novel shorted rectangular-loop antenna for circularly polarized wave operations," *Journal of Electromagnetic Waves and Applications*, Vol. 23, No. 10, 1323–1334, 2009.
9. Bai, X., X.-M. Zhang, L. Li, Q. Yang, and J. Li, "Double-sided printed four rhombic-loop antenna with parasitic loops

for circular polarization," *Journal of Electromagnetic Waves and Applications*, Vol. 23, No. 13, 1795–1802 2009.

10. Sze, J. Y., C.-I. G. Hsu, M. H. Ho, Y. H. Ou, and M. T. Wu, "Design of circularly polarized annular-ring slot antennas fed by a double-bent microstripline," *IEEE Trans. Antennas Propagat.*, Vol. 55, No. 11, 3134–3139, Nov. 2007.
11. Kumar, C. K. and S. N. Sinha, "A patch-loaded ring-slot antenna for wide band circular polarization," *Journal of Electromagnetic Waves and Applications*, Vol. 23, Nos. 17–18, 2409–2419, 2009.
12. Deng, S.-M., C.-L. Tsai, M.-F Chang, and S.-S. Bor, "A study on the non-uniform rectangular-ring slot antenna for broadband circular polarization operations," *Journal of Electromagnetic Waves and Applications*, Vol. 24, No. 4, 543–555, 2010.
13. Tseng, L. Y. and T. Y. Han, "Microstrip-fed circular slot antenna for circular polarization," *Microwave Opt. Technol. Lett.*, Vol. 50, No. 4, 1056–1058, Apr. 2008.
14. Han, T. Y., Y. Y. Chu, L. Y. Tseng, and J. S. Row, "Unidirectional circularly-polarized slot antennas with broadband operation," *IEEE Trans. Antennas Proporgat.*, Vol. 56, 1777–1780, Jun. 2008.
15. Row, J. S. and S. W. Wu, "Circularly-polarized wide slot antenna loaded with a parasitic patch," *IEEE Trans. Antennas Propagat.*, Vol. 56, 2826–2832, Sep. 2008.
16. Joseph, R., S. Nakao, and T. Fukusako, "Circular slot antennas using *L*-shaped probe for broadband circular polarization," *Progress In Electromagnetics Research C*, Vol. 18, 153–168, 2011.
17. Joseph, R. and T. Fukusako, "Bandwidth enhancement of circularly polarized square slot antenna," *Progress In Electromagnetics Research B*, Vol. 29, 233–250, 2011.
18. Sze, J. Y., J. C. Wang, and C. C. Chang, "Axial-ratio bandwidth enhancement of asymmetric-CPW-fed circularly-polarised square slot antenna," *IEE Elect. Lett.*, Vol. 44, No. 18, 1048–1049, Aug. 2008.
19. Sze, J. Y. and C. C. Chang, "Circularly polarized square slot antenna with a pair of inverted-L grounded strips," *IEEE Antenna and Wireless Propagat. Lett.*, Vol. 7, 149–151, 2008.
20. Chu, Q. X. and S. Du, "A CPW-fed broadband circularly polarized square slot antenna," *Microwave Opt. Technol. Lett.*, Vol. 52, 409–412, Feb. 2010.
21. Sze, J. Y., C. I. G. Hsu, Z. W. Chen, and C. C. Chang, "Broadband CPW-fed circularly polarized square slot antenna

with lightening-shaped feedline and inverted-L grounded strips," *IEEE Trans. Antennas Propagat.*, Vol. 58, 973–977, Mar. 2010.

22. Liao, W. and Q.-X. Chu, "CPW-fed square slot antenna with lightening-shaped feedline for broadband circularly polarized radiation," *Progress In Electromagnetics Research Letters*, Vol. 18, 61–69, 2010.